This article appeared in *Journal of Applied Physics 123, 105108 (2018);* and may be found at: https://doi.org/10.1063/1.5008368

Analysis of the magnetic properties in hard-magnetic nanofibers composite

R. Murillo-Ortíz, M. Mirabal-García, J. M. Martínez-Huerta, J. G. Cabal Velarde, I. E. Castaneda-Robles, and A. Lobo-Guerrero

Citation: Journal of Applied Physics **123**, 105108 (2018); doi: 10.1063/1.5008368
View online: https://doi.org/10.1063/1.5008368
View Table of Contents: http://aip.scitation.org/toc/jap/123/10
Published by the American Institute of Physics

Analysis of the magnetic properties in hard-magnetic nanofibers composite

R. Murillo-Ortíz,[1] M. Mirabal-García,[1] J. M. Martínez-Huerta,[2] J. G. Cabal Velarde,[3] I. E. Castaneda-Robles,[4] and A. Lobo-Guerrero[4,a)]

[1]*Instituto de Física, Universidad Autónoma de San Luis Potosí, Álvaro Obregón No. 64, Zona centro, 78000 San Luis Potosí, S.L.P., Mexico*

[2]*División de Materiales Avanzados, Instituto Potosino de Investigación Científica y Tecnológica, Camino a la Presa de San José 2005, 78216 San Luis Potosí, S.L.P., Mexico*

[3]*Instituto Tecnológico Superior de Irapuato, Carretera Irapuato-Silao Km 12.5, 36821 Irapuato, Guanajuato, Mexico*

[4]*Instituto de Ciencias Básicas e Ingeniería, Universidad Autónoma del Estado de Hidalgo. Carr. Pachuca-Tulancingo Km. 4.5, Col. Campo de Tiro, 42039 Mineral de la Reforma, Mexico*

(Received 5 October 2017; accepted 1 March 2018; published online 14 March 2018)

The magnetic properties of the strontium hexaferrite nanoparticles were studied as they were embedded at different concentrations in poly(vinyl alcohol) (PVA) nanofibers. These nanoparticles were prepared using the Pechini method and a low frequency sonication process obtaining a 3.4 nm average diameter. The composite consisting of hard magnetic nanoparticles homogeneously dispersed in a polymeric matrix was fabricated using a homemade electrospinning with 25 kV DC power supply. The obtained nanofibers had an average diameter of 110 nm, and nanoparticles were arranged and distributed within the nanofibers under the influence of a strong electric field. The configuration of the magnetic nanoparticles in the PVA nanofibers was such that the interparticle exchange interaction became negligible, while the magnetostatic interaction turned out predominant. The results reveal a considerable improvement in the energy product (BH_{max}) and in the squareness ratio (M_r/M_s) for nanoparticle concentrations between 15 and 30% per gram of PVA. The nanoparticles arrangement occurred at densities below the percolation concentration enhanced the hard-magnetic properties of the nanofibers, which indicates that the organization of the particles along the fibers induces anisotropy from the magnetostatic interaction among the magnetic nanoparticles. Finally, we close the discussion analyzing the observed effect below the percolation threshold, where the induced anisotropy caused the reduction of the full-width at half-maximum of the switching field distribution curves. *Published by AIP Publishing.*
https://doi.org/10.1063/1.5008368

I. INTRODUCTION

Hexagonal ferrites (hexaferrites) are one of the most important hard magnetic materials used in current technology. Since their discovery in the Philips laboratories more than 60 years ago, these compounds have been closely linked to the development of information storage technology, microwave sensors, DC motors, etc.[1] Hexaferrites are iron based compounds formed from close-packed oxygen anions, in which one O^{2-} anion is substituted with one alkaline earth metal cation (Me = Ba, Sr, Pb), and the iron cations occupy the interstitials positions, preserving the structural skeleton of the magnetoplumbite mineral. The hexaferrite unit cell has 64 ions located on 11 different symmetry sites, the 24 iron cations are distributed over five distinct sublattices, three octahedral (12k, 2a, and $4f_2$), one tetrahedral ($4f_1$), and one bipyramidal (2b). This compound crystallizes in the $P6_3/mmc$ space group showing ferrimagnetic ordering of the iron magnetic moments.

Hexaferrites are currently an important component in numerous technological devices, mainly due to their hard-magnetic properties, exhibiting large magnetocrystalline anisotropy, moderate energy product, high Curie temperature, and strong corrosion resistance.[2,3] Also, they exhibit magnetoelectric,[4] multiferroic,[5] and dielectric properties.[6] All these properties show that hexaferrites are interesting for a great variety of applications, stand out permanent magnets,[7] magnetic recording media, data storage technology,[8] electromagnetic interference suppressors,[9] high frequency filters,[10] and some other novel applications.[11,12] Interaction effects between particles become important for data storage applications since one bit is defined in terms of the hysteresis properties. Then, each particle needs to have large remanent magnetization (M_r) to ensure the information integrity, low magnetization saturation (M_s), and low coercivity (H_c) so that re-recording can be performed using small magnetic fields. These properties can be designed in a wide value range by varying intrinsic and extrinsic parameters of the hexaferrite compounds such as their chemical composition and morphology.[13–16] However, the problem of high noise levels in magnetic recording media has been associated with the magnetic interactions between particles.[17] If these interactions become strong enough, writing one stable bit by

a)Author to whom correspondence should be addressed: azdlobo@gmail.com. Present address: Área Académica de Ciencias de la Tierra y Materiales, Universidad Autónoma del Estado de Hidalgo, Carr. Pachuca-Tulancingo Km. 4.5, Col. Campo de Tiro, 42039 Pachuca de Soto, Mexico.

switching the magnetization state of one particle is too difficult. In this sense, it is widely known that interparticle interactions play a significant role in determining the magnetic properties.

Several methods have been proposed to characterize the magnetic interactions, such as the δM method based on the Stoner-Wohlfarth model,[18] and the first-order reversal curves (FORCs) method based on the phenomenological Preisach–Néel theory of hysteresis.[19,20] Although both methods can evaluate the interaction state of a set of magnetic particles, they present some drawbacks. One is related to restrictions on the particle characteristics (uniaxial, mono-domain, and so on), and the other one is related to highly interacting systems interpretation, as well as lack of clarity to recognize the interaction type.[21] Another method for the magnetic interactions study is the differential susceptibility of the demagnetization branch, also called switching field distribution (SFD). This is a micromagnetic characteristic curve used to evaluate the breadth of the distribution field at which reversal magnetization occurs.[22] In contrast with the FORC diagram and the δM curve, the SFD curve can be easily obtained from the direct differentiation of the demagnetizing branch.[23,24] That places the SFD as a simple and accessible way to assess the intensity and the interaction type.

In a system composed of magnetic nanoparticles arranged far apart (diluted system), the coercive field of one particle is independent of the others, and considering that particles are not completely identical, the full system is characterized by having a certain distribution of the coercive fields, called intrinsic switching field distribution (iSFD). In this case, such distribution is accessed as the derivative of a branch of hysteresis loop. On the other hand, if the nanoparticles are arranged close together without having contact, the field produced by each particle begins to interfere with that of neighboring particles. In this system, the coercive field distribution becomes enlarged due to dipolar interaction, and a larger magnetic field is required to switch the entire set of particles; this broadens the SFD and, therefore, enlarges the full-width at half-maximum (FWHM) as magnetostatic interactions become stronger.[25,26] For particle systems with the same iSFD, relative changes in FWHD denotes a measure of magnetostatic interactions.

In this work, the magnetic properties of strontium hexaferrite nanoparticles (SrM-NPs) embedded in poly(vinyl alcohol) (PVA) nanofibers have been investigated at different nanoparticle concentrations in the PVA matrix. These nanoparticles were distributed along the z-axis of the PVA nanofibers because of the strong interaction with the electric field during the electrospinning experiment. The ability to configure magnetic nanoparticles in a polymeric matrix makes this system an interesting model with multiple experimental options to investigate the role of interparticle interactions on magnetic properties when the nanoparticle concentrations vary below the percolation threshold.[27] The percolation limit is defined as the concentration at which each magnetic site has, at least, one magnetic nearest neighbor. Thus, a direct interaction can be uninterruptedly established through the whole sample. Changing the concentration of the SrM-NPs below the percolation threshold, these nanostructured composites show interesting effects, for example, a meaningful increase on the remanence, energy product, and coercivity field, with respect to the bulk SrM-NPs nanoparticles. In addition, this system presents a narrowest SFD curve when nanoparticle concentration increases, such behavior can largely be attributed to the formation of an increasing anisotropy that originates from the magnetostatic interaction among the nanoparticles.[28]

II. EXPERIMENTAL

The Pechini method was used to prepare the strontium hexaferrite nanoparticles. 4.5 g of ferric nitrate $[Fe(NO_3)_3{\cdot}9H_2O]$ was mixed with 0.19 g of strontium nitrate $[Sr(NO_3)_2]$ and stirred in 60 ml of deionized water at room temperature for 30 min, and 1.0 g of citric acid ($C_6H_8O_7$) and 0.25 ml of ethylene glycol ($C_2H_6O_2$) were incorporated into 10 ml of deionized water; both solutions were mixed and stirred at 70 °C until water evaporates to promote a polyesterification reaction. The organic matrix containing metallic ions was heated at 200 °C for 4 h and then the obtained powder was sintered at 900 °C maintaining this temperature for 2 h. The nanoparticles were put into an alcoholic medium, and they were sonicated for 1 h in the ultrasonic bath at 40-kHz, to disperse, deagglomerate, and fragment the nanoparticles. For the polymeric matrix, 0.75 g of PVA (MW = 75 000) was dissolved in 25 ml of deionized water. The mixture was stirred slowly for 40 min at 80 °C, and it was left to rest at room temperature. Four samples with different SrM-NPs (900 °C) concentrations were considered. The PVA-SrM nanofibers were fabricated using 0.15 g, 0.20 g, 0.25 g, and 0.30 g of SrM-NPs per gram of PVA; these samples were labelled as 15%, 20%, 25%, and 30%, which correspond to the nanoparticle percentage in each sample, respectively. Additionally, one sample with 10% of SrM-NPs was fabricated to observe the effect of low SrM-NP concentration. As shown later, for SrM-NPs below 15%, the relatively low concentration results in a fall of the magnetic properties. For concentrations above 30%, the polymeric mix became too viscous and its ejection through the needle was difficult in our system.

A syringe with a 0.15 mm internal diameter stainless-steel needle was filled with the ultrasonicated PVA mix containing the SrM-NPs. Afterwards, the loaded syringe was placed in an infusion pump programmed to deliver a flow rate of 0.3 ml/h through the thin nozzle, which serves as an electrode (anode). The stationary target or collector screen (cathode) was an aluminum plate at 5.3 cm from the syringe tip, and then a high electric field was applied with a high voltage DC power supply that we have constructed for the electrospinning experiments. This high voltage supply is a single phase full-wave rectification system that works in a switching mode, where the chopper circuit switches the resultant high voltage at a frequency of 10 kHz through a light weight transformer. The power supply delivers an output voltage that remains close to its rating within 1%, and the residual high frequency voltage ripple at 25 kV is about

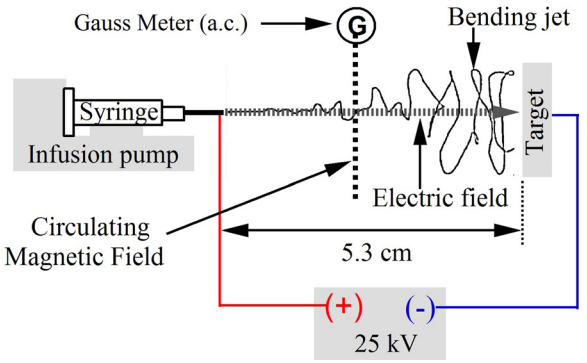

FIG. 1. Schematic configuration of the electrospinning system for the fabrication of PVA nanofibers with embedded hexaferrite nanoparticles.

0.6%. The electric potential difference between the needle tip and the collector screen was adjusted to 25 kV although at low SrM-NPs concentration it is possible to use smaller potentials. Since a certain amount of an AC component is superimposed on the high DC voltage, we have used a Bell-5180 Gauss/Tesla meter provided with a transverse probe, model number (5180): STD18–0404, with the purpose of trying to detect and measure the possible presence of a magnetic flux, due to the electric field fluctuations produced with the power supply during the electrospinning process. As once suggested by Warner *et al.* in a previous study.,[29] Figure 1 shows the schematic fabrication setup of the nanofibers done by electrospinning.

The crystallinity of the strontium hexaferrite nanoparticles was studied for various sintering temperatures ranging from 750 °C to 900 °C using a Bruker D8 Advance diffractometer with CuK_{α} radiation ($\lambda = 1.54$ Å). Nanoparticle arrangement and morphologic characteristics of the nanofibers composite were studied with a Hitachi S-570 transmission electron microscope (TEM) working at 100 kV. The magnetic properties were obtained from the hysteresis loop at room temperature with a LDJ-9600 vibrating sample magnetometer (VSM). The SFD curves were obtained from the first derivative of the demagnetizing branch of the hysteresis loops.

III. RESULTS AND DISCUSSION

Figure 2 shows the magnetic and structural characterization of the strontium hexaferrite nanoparticles at various sintering temperatures, (a) 750 °C, (b) 800 °C, (c) 850 °C, and (d) 900 °C. Each experimental X-ray pattern is presented with its corresponding Rietveld refinement profile. The phases analysis and crystalline parameters were obtained using MAUD, a free access program for Rietveld refinement,[30] using hematite (trigonal, R-3c:H, a = 5.035, c = 13.748) and strontium hexaferrite (hexagonal, $P6_3/mmc$, a = 5.884; c = 23.050) as initial models. The magnetic characterization

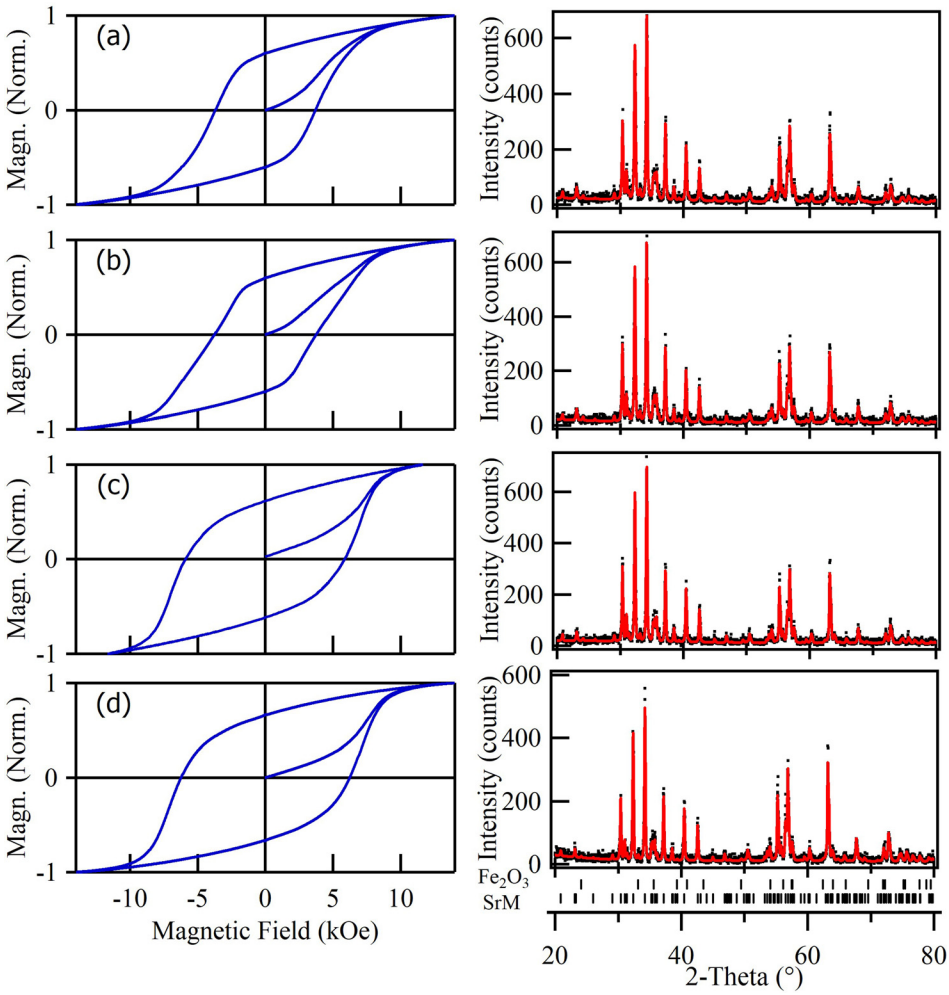

FIG. 2. Hysteresis loops of the strontium hexaferrite nanoparticles sintered at (a) 750 °C, (b) 800 °C, (c) 850 °C, and (d) 900 °C and their corresponding experimental (·) and calculated (—) X-ray diffractograms.

TABLE I. Magnetostructural characterization of nanoparticles obtained at various sintering temperatures before their sonication.

	Strontium hexaferrite phase							
Temperature (°C)	Lattice parameters (Å)	Volume (Å^3)	Cryst. size (nm)	Purity (wt. %)	χ^2	M_r/M_s (%)	H_c (kOe)	BH_{max} (MGOe)
750	a = 5.8790 (1) c = 23.0582 (15)	796.95	74 (1)	96.65	1.39	60	3.68	2.47
800	a = 5.8795 (4) c = 23.0588 (14)	797.11	82 (2)	96.80	1.42	60	3.75	2.41
850	a = 5.8804 (1) c= 23.0593 (13)	797.37	95 (3)	96.95	1.37	61	5.89	2.99
900	a = 5.8823 (1) c = 23.0642 (13)	798.05	103 (4)	98.20	1.38	63	6.30	3.01

was obtained from the hysteresis loops measured at room temperature.

Figure S1 shows a TEM micrograph of the SrM-NPs after they were sintered at 900 °C. The particle size showed in the TEM micrograph matches with the crystallite size obtained from the Rietveld method. According to the phase analysis, the sample sintered at 750 °C has 3.35% wt. of iron oxide (hematite) which decreases as sintering temperature increases. At 900 °C, the presence of iron oxide is 1.80% wt. Higher sintering temperature is not recommended due to grain growth and particle hardening, which makes its fragmentation difficult by sonication. Other observable effects of temperature on the crystalline structure are related with changes on the lattice distances and the crystallite's size. The quality of the Rietveld fit was evaluated from the Chi squared, $\chi^2 = (R_{wp}/R_{exp})^2$; these values together with the observed and calculated patterns indicate a good fit of the Rietveld analyses.[31] Table I shows the magnetostructural parameters for the hexaferrite nanoparticles at different sintering temperatures. Changes on the magnetic properties have been associated with morphological characteristics such as size and shape distributions, but also with changes occurring at structural level in the hexaferrite. Interatomic distances and unit-cell lengths play an important role in the configuration of the magnetic properties in these compounds. Figure 3 shows the behavior among the unit-cell volume and the coercivity of the strontium hexaferrite nanoparticles. In this sense, both parameters maintain a trend to increase with the sintering temperature increment.

The SrM-NPs sintered at 900 °C were used to fill the nanofibers due to their higher purity, and because they present a higher squareness ratio as well as a higher energy product than those values shown by the samples sintered at lower temperatures. The M_s value at maximum applied field for this sample, measured before defragmenting, was

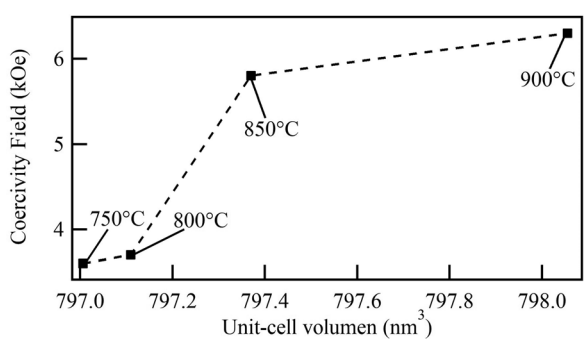

FIG. 3. Behavior of the coercive field with the unit-cell volume (dotted line is a guide for the eye).

72.2 emu/g with 14 kOe of applied field, which agrees with the expected M_s value for the SrM-NPs prepared by Pechini method.[32] The X-ray pattern of the SrM-NPs shown in Fig. S2 indicates a reduction of the crystallite size after powders were sonicated. Figure 4(a) shows TEM micrographs of the PVA-SrM nanofibers with an average diameter of 103 nm. In Fig. 4(b), SrM-NPs embedded in the PVA nanofibers is observed; these nanoparticles have uniform size; they are isolated, homogeneously distributed, and do not show presence of agglomerates. In Fig. 4(c), it is observed that nanoparticles are ordered on the surface and aligned with respect to the nanofibers' growth; this is the consequence of the nanoparticles' interaction with the highly intense electric field aligned with the electrodes in a point-plate configuration, where the electric field is applied between the capillary tip or needle at high electric potential and a grounded plate collector. At present, we cannot absolutely conclude whether the magnetic field surrounding the fiber jet, and which originated by the electric field fluctuations produced with the power supply, according to $\nabla \times \mathbf{H} = \partial D/\partial t$, i.e., the time-changing E-field between the tip of the needle and the stationary target as the fibers are ejected, has an influence on the distribution of the magnetic NPs in the nanofibers. This is shown in Fig. 1. However, further systematic experimental investigation in this direction is needed to gain a better understanding of this possible interaction.

As it has been proposed and discussed in previous electrospinning studies,[33] initially the droplet of the polymeric solution that has been pumped through the thin nozzle to the syringe tip is held by its surface tension, and the magnetic nanoparticles are homogeneously distributed. But after applying a high voltage to the nozzle that serves as an electrode, charge is induced on the fluid surface and the droplet is distorted. As the voltage increases above a critical value, a single jet is ejected from the apex of a cone-shaped deformation, referred to as the Taylor cone,[34] and moves towards the collector plate. It thins rapidly with the distance and due to repulsive forces, ions and the charged magnetic NPs move radially to the jet surface.[35] When the concentration of ions and nanoparticles at the jet surface reaches a critical value, solvent evaporates, and the jet is converted into solid nanofibers via whipping instability the fiber polymerizes during its path to the target and the nanoparticles get arrested and fixed inside the matrix and precipitate onto the stationary collector screen. The arrangement of the magnetic particles was observed uniformly distributed inside the surface of the nanofibers' composite and show no agglomeration, as shown in Figs. 4(b) and 4(c).

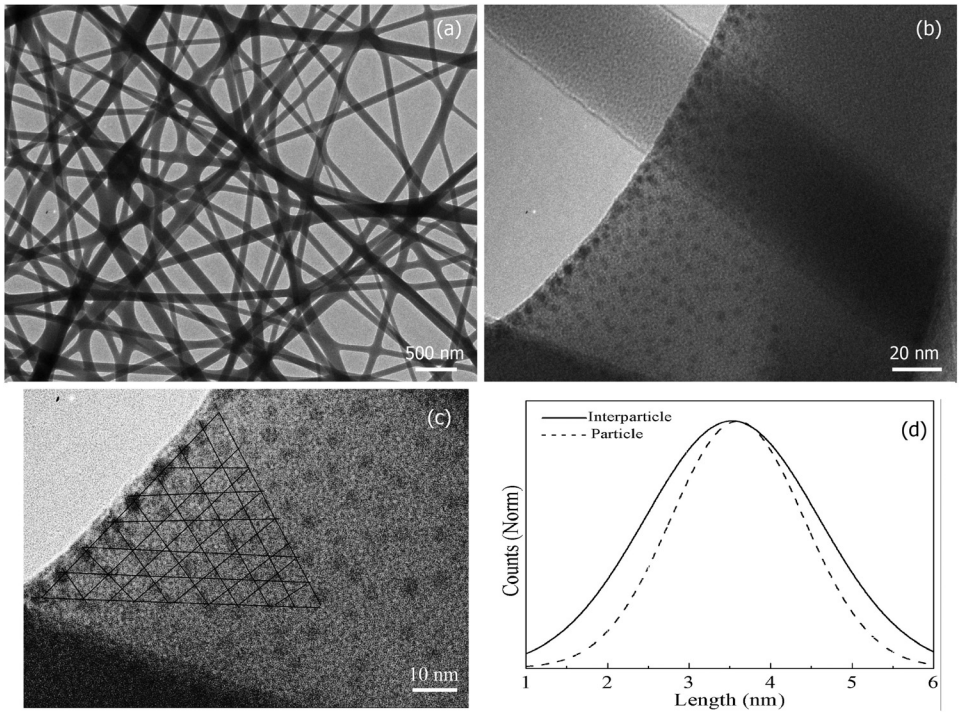

FIG. 4. TEM micrographs show (a) the nanofibers composite, (b) the SrM-NPs embedded in the PVA matrix, and (c) the magnetic nanoparticles arrangement. (d) Particle size distribution (dashed line) and interparticle first neighbors distance (solid line).

The magnetic field was measured with the above described Gaussmeter, scanning all the space near the jet trajectory with the Hall-effect sensor, by avoiding contact with the jet, from the region where the cone-shaped deformation of the polymer solution takes place to the whipping instability zone. The transverse probe was oriented in all directions registering the AC and DC magnetic field in the DC and AC mode, resulting in the following: It was impossible to measure a stable DC magnetic field due to strong fluctuations; however, it was possible to measure a stable AC magnetic field circulating about the jet direction, only in the middle of the fiber path before reaching the cathode, i.e., at 2.65 cm from the needle tip. The magnetic field surrounds the jet trajectory in concentric circles and an average AC field of 0.35 mT (3.5 G) was obtained when the Hall sensor was correctly oriented and positioned at a radius of 1.08 cm above the horizontal line joining the needle tip and the target, in the middle of the fiber path before reaching the cathode. It was found that this azimuthal field varies approximately with the circle radius according to Ampere's law, corroborating the presence of a displacement current due to the electric field fluctuations produced with the power supply during the electrospinning. Thus, it is predictable that the field strength increases near the nanofiber surface. An average background AC field of 0.21 mT (2.1 G) was measured *in situ*.

The average particle size as well as the interparticle distances to first neighbors was measured from TEM micrographs using ImageJ, an open program for image analysis. Figure 4(d) shows that the nanoparticle size distribution is centered at 3.4 nm and the interparticle distribution lengths in 3.5 nm for sample with 25% of nanoparticles. According to the above previous discussion, it is fully expected that interparticle distances decrease as nanoparticles concentration increases.

Figure 5 shows the normalized hysteresis loops of the nanofiber composite compared with the one obtained from the nanoparticles sintered at 900 °C. It is observed that the hard-magnetic properties of the nanofibers have been improved with respect to those measured for SrM-NPs. The magnetic behavior of the nanofibers is closely dependent on the SrM-NPs concentration, when the concentration goes from 15% to 30%; the coercivity field rises from 6.3 to 6.6 kOe, and the squareness ratio increases from 71% to 81%. The sample with 30% of SrM-NPs presents one of the highest squareness ratio reported in literature for hexaferrite nanoparticles.[36,37] Typical squareness ratio for randomly oriented hexaferrite is around 50%,[38] and only Sr-hexaferrite thin films with perpendicular magnetization have a squareness ratio of 96%.[39]

Figure 6(a) shows the squareness ratio and coercivity versus the SrM-NPs concentration. Results in the range of $0.15 < x < 0.30$ show a trend to increase the remanent magnetization as well as the coercitive field when the nanoparticle concentration increases. However, M_r/M_s and H_c are usually found to decrease because of the magnetostatic

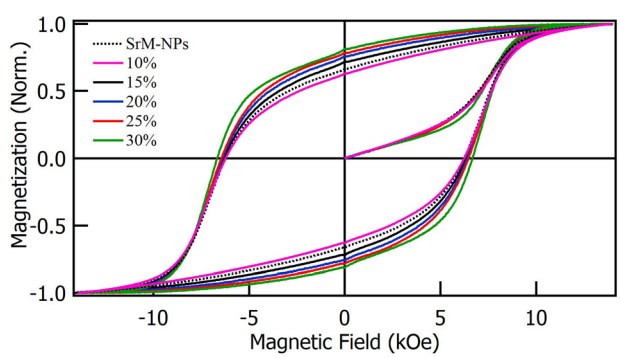

FIG. 5. Hysteresis loops obtained from the nanofibers at different nanoparticles concentration. Dotted line corresponds to the SrM-NPs sintered at 900 °C.

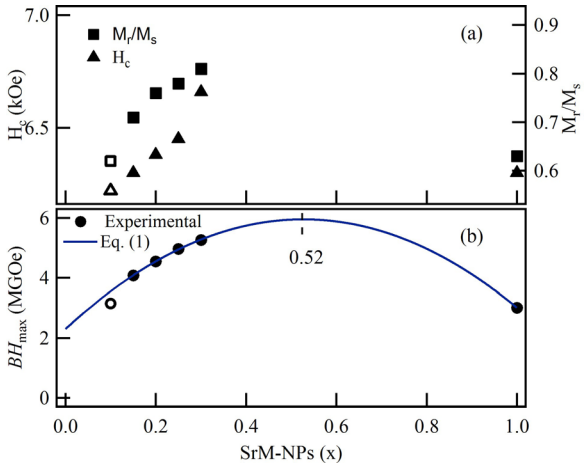

FIG. 6. (a) Behavior of the coercivity field and squareness ratio; (b) energy product versus the SrM-NPs concentration (x), for the investigated nanofibers.

interactions.[40] Recent investigations on SrM nanomagnets found upper coercivity field and saturation magnetization; however, the squareness ratio remains on 0.55.[41] This behavior is attributable to a strong influence of the magnetostatic interparticle interactions. The PVA-SrM nanofibers investigated in this work tend to increase the squareness ratio when SrM-NPs concentration increases; this behavior is explained as result of an induced anisotropy originated from the arrangement of nanoparticles in the PVA nanofibers. The induced anisotropy depends on the nanoparticle's characteristics and their spatial arrangement because of its magnetostatic origin. Under this scenario, there exists a competition between uniaxial anisotropy with magnetizing effect and the magnetostatic field, obtaining maximum magnetization before reaching the percolation threshold.[28] The energy stored in a hard-magnet depends on its coercivity and magnetization remanence; nonetheless above the percolation threshold, the energy product is limited by creation of magnetostatic fields.[42] Figure 6(b) shows a remarkable increment in the BH_{max} product with the nanoparticle concentration. PVA-SrM nanofibers with 15% of SrM-NPs present a BH_{max} increment of 35%, whilst the sample with 30% of SrM-NPs has the highest increment, reaching 75% more BH_{max} than the sample obtained from the SrM-NPs sintered at 900 °C. The behavior of the energy product with the concentration of nanoparticles (x) has been fitted through the following equation:

$$BH_{max}(x) = 2.30 + 13.85x - 13.14x^2. \quad (1)$$

This relation describes a parabola wherein the BH_{max} of the SrM-NPs powder corresponds to $x = 1.0$, and according to this fitting, the maximum BH_{max} of the composite is obtained at $x = 0.52$, reaching up to 97% more BH_{max} than the one obtained from the bare SrM-NP powder. It is expected that above this point, the energy product decreases as SrM-NP concentration increases due to an increase in the demagnetizing effects and because by reaching the percolation limit, the order that produces the anisotropy decreases. According to the obtained results, the quadratic tendency in Eq. (1) is phenomenological. In a magnet, the induction depends on internal field, which in turn depends on external and demagnetizing fields. Now, demagnetizing field is defined in terms of the magnet shape and how the magnetostatic charges are distributed on its surface. A nanostructured magnet, such as the one obtained in this case, increases the available surface area and the demagnetizing field can be modulated through the nanoparticle concentration, and hence its BH_{max}. An increasing BH_{max} is expected for an anisotropic configuration of the particles inside of a magnet; however, when the number of particles is very low, the amount of magnetic material available decreases more than necessary and with it the BH_{max}. A reduction on the SrM-NPs concentration ($x \leq 0.1$) generates a drop in the magnetization of the system and therefore, the energy product cannot be accurately described from Eq. (1), as the unfilled marks of Fig. 6 confirm for one sample with $x = 0.1$. However, at intermediate compositions, this parabolic behavior represents a good approximation. Additionally, the concentration at which Eq. (1) reaches its maximum has been associated with the magnetic arrangement of the nanoparticles. Conversely, if nanoparticles form a chaotic system with random nanostructures, the BH_{max} peak should be found at lower concentrations.[40] Then, considering that there are no exchange interactions, the increased BH_{max} is the result of an anisotropy field which emerges from the magnetostatic effects between particles.[40,43,44] In this case, the long-range influence of the magnetostatic field promotes a collaborative process that increases the energy product although this behavior is closely linked with the spatial configuration of nanoparticles.

Figure 7 shows the SFD curves of the nanofibers composites at various SrM-NPs concentrations between 15 and 30%. It is observed that the FWHM of the SFD has a trend to decrease when nanoparticle concentration increases. For nanofibers with 15% of magnetic nanoparticles, the FWHM measured was 3.24 kOe, while for a nanoparticle concentration of 30%, the FWHM falls to 2.68 kOe. The interaction field has been related qualitatively with the FWHM width of the SFD curve. A broader FWHM has been related to a system with high magnetostatic interaction. Then a wider SFD would be expected as the concentration of particles increases. However, this is only the case when particles are randomly ordered inside the polymer. When particles are arranged along the nanofibers, the magnetostatic energy is minimized as the magnetic field generated by particles produces field lines that tend to be parallel to the axis of the fiber rather than perpendicular to it. In this case, a ferro-type interaction is favored and neighboring particles orientate along the same direction, turning this into an easy axis of magnetization. Then, the results exhibited in the studied nanofibers are consistent with the development of a magnetic anisotropy originated from the magnetostatic interactions in a set of ordered magnetic nanoparticles and fixed in a nonmagnetic matrix. It has been noticed how the magnetic dipolar anisotropy is related to the matrix shape and the way nanoparticles are arranged within it.[45]

The nanoparticles arrangement plays an important role in the configuration of the magnetostatic field and the subsequent improvement of the hard-magnetic properties. Table II

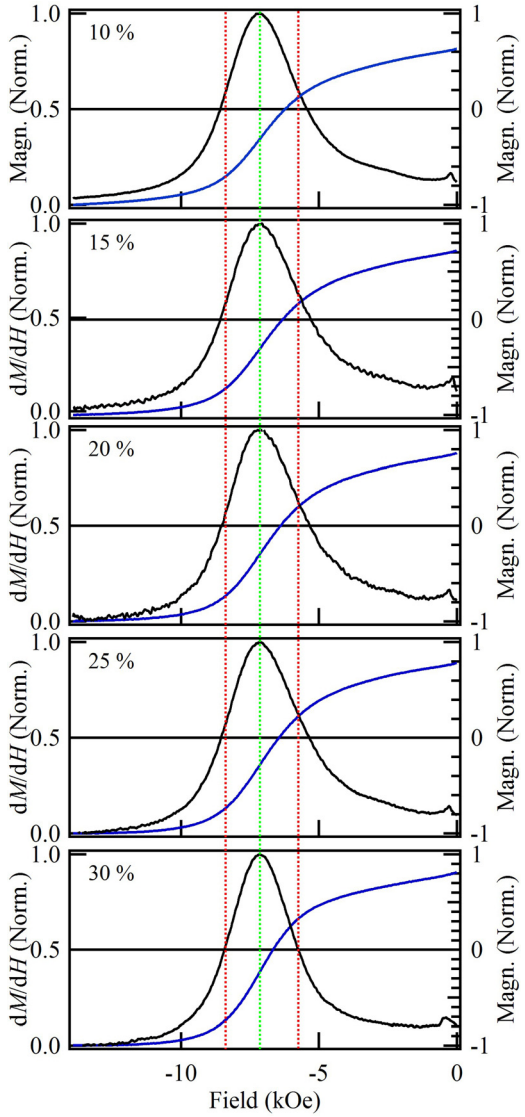

FIG. 7. SFD curves of the nanofibers composites at various SrM-MPs concentrations (black line). The demagnetizing branch is indicating the squareness ratio at null field (blue line). Dotted and dashed lines are guides for the eye.

summarizes the magnetic parameters obtained from the nanofibers composites. An improvement of the hard-magnetic properties according with the increase of the magnetic nanoparticles density is observed. This behavior has been previously detected in nanowires where the energy product increases to reach a maximum when the packing fraction increases.[40]

TABLE II. Magnetic characterization of SrM-NP nanofibers at various SrM-NP concentrations.

SrM-NPs (%)	M_r/M_s (%)	H_c (kOe)	BH_{max} (MGOe)	ΔBH_{max} (%)	SFD_{FWHM} (kOe)	SFD_{Center} (kOe)
10	63	6.22	3.23	6	3.22	7.184
15	71	6.30	4.08	35	3.24	7.103
20	76	6.38	4.55	51	3.19	7.140
25	78	6.45	4.97	65	2.99	7.129
30	81	6.66	5.26	75	2.68	7.122

The demagnetizing field strength in an assembly of magnetic nanoparticles depends on the size, arrangement, and concentration of nanoparticles. In this case, due to the arrangement of the magnetic nanoparticles fixed inside the surface of the PVA nanofibers below the percolation threshold, the demagnetizing effects were reduced by the development of a magnetic anisotropy of magnetostatic nature, resulting in an improvement of the energy product in the composite. These induced improvements on the magnetic properties of the hexaferrite as part of a polymeric composite offer the possibility of studying some important mechanisms concerning magnetic interactions, anisotropy, and dilution effects that could have potential applications in technological devices which demand high magnetic performance, low fabrication costs, or functional properties. On the other hand, the relation among the magnetostatic field with the observed improvement of its magnetism needs to be further studied to take advantage of the anisotropic properties presented in nanostructured composites.

IV. CONCLUSION

A magnetic composite with high hard-magnetic performance was developed from hexaferrite nanoparticles embedded in polymer nanofibers. These magnetic nanoparticles were ordered in the nanofibers as a result of the nanoparticle's interaction with the applied electric field, during the electrospinning. The obtained nanofiber composites present a maximum improvement of 70% of the energy product, 35% of squareness ratio, and 5% in coercivity with respect to the SrM-NPs powder. Although these values are dependent on the concentration of nanoparticles, all the studied concentrations exceed the efficiency present in the SrM-NPs alone. The improvement on the hard-magnetic properties of the composite is because of the emergence of an anisotropy field that is dependent on the magnetostatic interaction field.

SUPPLEMENTARY MATERIAL

See supplementary material for two figures. Figure S1 shows a TEM micrograph of SrM-NPs, while Fig. S2 shows the X-ray diffractogram after nanoparticles were exposed to the sonication process.

ACKNOWLEDGMENTS

Authors thank G.G. López Rocha (IF-UASLP) for his lab assistance and Carolina Medina (IF-UASLP) for her critical reading and comments on the manuscript. R.M.-O. thanks CONACYT 240837 scholarship and A.L.-G. thanks UAEH/PRODEP-México for partial support through the Contract No. 511-6/17-8021.

[1]M. Sugimoto, J. Am. Ceram. Soc. **82**, 269 (1999).
[2]R. Valenzuela, *Magnetic Ceramics* (Cambridge University Press, New York, 1994).
[3]B. D. Cullity and C. D. Graham, *Introduction to Magnetic Materials* (IEEE Press, New Jersey, 2009).
[4]Y. A. Hamam, M. R. Said, and I. Abu-Aljarayesh, Physica B **321**, 129 (2002).
[5]G. Tan and X. Chen, J. Magn. Magn. Mater. **327**, 87 (2013).

[6]A. Arora and S. B. Narang, J. Mater. Sci.: Mater. Electron. **27**, 10157 (2016).
[7]R. Skomski and J. M. D. Coey, Scr. Mater. **112**, 3 (2016).
[8]O. Shimizu, M. Oyanagi, A. Morooka, M. Mori, Y. Kurihashi, T. Tada, H. Suzuki, and T. Harasawa, J. Magn. Magn. Mater. **400**, 365 (2016).
[9]R. Valenzuela, Phys. Res. Int. **2012**, 591839.
[10]S. B. Narang, P. Kaur, and S. Bahel, Mater. Sci.-Pol. **34**, 19 (2016).
[11]A. A. Farghali, M. H. Khedr, and A. F. Moustafa, Mater. Technol.: Adv. Perform. Mater. **23**, 104 (2008).
[12]G. H. Lim, J. Lee, N. Kwon, S. Bok, H. Sim, K. S. Moon, S. E. Lee, and B. Lim, Electron. Mater. Lett. **12**, 574 (2016).
[13]G. Litsardakis, I. Manolakis, and K. Efthimiadis, J. Alloys Compd. **427**, 194 (2007).
[14]S. Ounnunkad, Solid State Commun. **138**, 472 (2006).
[15]A. L. Guerrero, M. Mirabal-García, S. A. Palomares-Sánchez, and J. R. Martínez, J. Magn. Magn. Mater. **399**, 41 (2016).
[16]A. L. Guerrero-Serrano, M. Mirabal-García, and S. A. Palomares-Sánchez, J. Supercond. Novel Magn. **27**, 1709 (2014).
[17]X. He, C. Alexander, Jr., and M. R. Parker, IEEE Trans. Magn. **28**, 2683 (1992).
[18]E. C. Stoner and E. P. Wohlfarth, Philos. Trans. R. Soc. London, Ser. A **240**, 599 (1948).
[19]L. Néel, Appl. Sci. Res., Sect. B **4**, 13 (1954).
[20]F. Preisach, Z. Phys. **94**, 277 (1935).
[21]A. D. Volodchenkov, Y. Kodera, and J. E. Garay, J. Mater. Chem. C **4**, 5593 (2016).
[22]N. Kodama, H. Inoue, G. Spratt, Y. Uesaka, and M. Katsumoto, J. Appl. Phys. **69**, 4490 (1991).
[23]A. Berger, Y. H. Xu, B. Lengsfield, Y. Ikeda, and E. E. Fullerton, IEEE Trans. Magn. **41**, 3178 (2005).
[24]A. Berger, B. Lengsfield, and Y. Ikeda, J. Appl. Phys. **99**, 08E705 (2006).
[25]R. W. Chantrell and K. O'Grady, J. Phys. D: Appl. Phys. **25**, 1 (1992).
[26]R. Proksch and B. Moskowitz, J. Appl. Phys. **75**, 5894 (1994).
[27]T. J. Fiske, H. S. Gokturk, and D. M. Kalyon, J. Mater. Sci. **32**, 5551 (1997).
[28]D. Kechrakos and K. N. Trohidou, Phys. Rev. B **58**, 12169 (1998).
[29]S. B. Warner, A. Buer, M. Grimler, S. C. Ugbolue, G. C. Rutledge, and M. Y. Shin, National Textile Center Annual Report No. M98-D01 (1999).
[30]L. Lutterotti, S. Matthies, H.-R. Wenk, A. J. Schultz, and J. Richardson, J. Appl. Phys. **81**, 594 (1997).
[31]B. H. Toby, Powder Diffr. **21**, 67 (2006).
[32]A. E. Ramirez, N. J. Solarte, L. H. Singh, J. A. H. Coaquira, and S. Gaona, J. Magn. Magn. Mater. **438**, 100 (2017).
[33]Y. M. Shin, M. M. Hohman, M. P. Brenner, and G. C. Rutledge, Polymer **42**, 9955 (2001).
[34]G. I. Taylor, Philos. Trans. R. Soc. London, Ser. A **280**, 383 (1964).
[35]B. Yalcinkaya, F. Yener, O. Jirsak, and F. Cengiz-Callioglu, J. Nanomater. **2013**, 538179.
[36]M. N. Ashiq, A. S. Asi, S. Farooq, M. Najam-ul-Haqa, and S. Rehman, J. Magn. Magn. Mater. **444**, 426 (2017).
[37]B. Abraime, M. Ait Tamerd, A. Mahmoud, F. Boschini, A. Benyoussef, M. Hamedoun, Y. Xiao, A. El Kenz, and O. Mounkachi, Ceram. Int. **43**, 15999 (2017).
[38]Y. Chen, T. Sakai, T. Chen, S. D. Yoon, A. L. Geiler, C. Vittoria, and V. G. Harris, Appl. Phys. Lett. **88**, 062516 (2006).
[39]X. S. Liu, B. X. Gu, W. Zhong, H. Y. Jiang, and Y. W. Du, Appl. Phys. A **77**, 673 (2003).
[40]S. Gangopadhyay, G. C. Hadjipanayis, C. M. Sorensen, and K. J. Klabunde, IEEE Trans. Magn. **29**, 2619 (1993).
[41]P. Jing, J. Du, J. Wang, J. Wei, L. Pan, J. Li, and Q. Liu, Sci. Rep. **5**, 15089 (2015).
[42]R. Skomski, Y. Liu, J. E. Shield, G. C. Hadjipanayis, and D. J. Sellmyer, J. Appl. Phys. **107**, 09A739 (2010).
[43]W. C. Chang, D. Y. Chiou, S. H. Wu, B. M. Ba, and C. O. Bounds, Appl. Phys. Lett. **72**, 121 (1998).
[44]A. M. Gabay, M. Marinescu, and G. C. Hadjipanayis, J. Appl. Phys. **99**, 08B506 (2006).
[45]J. M. Martinez-Huerta, J. De La Torre Medina, L. Piraux, and A. Encinas, J. Phys.: Condens. Matter **25**, 226003 (2013).